High-precision measurement of the $2s2p\ ^1P_1^o$ center of gravity in neutral ^{9}Be at the parts-per-billion level

K. J. Ahrendsen, E. M. Kay, and W. D. Williams*
Physics Department, Smith College, Northampton, Massachusetts 01063, USA

(Received 30 May 2025; accepted 9 July 2025; published 23 July 2025)

We use saturated absorption spectroscopy to study neutral ^{9}Be atoms produced in a dc discharge lamp. Previous measurements of the $2s2p\ ^1P_1^o$ state energy were limited in precision due to overlapping hyperfine structure. In this work, we apply a 400 G magnetic field, which splits the magnetic sublevels creating a spectral feature near the center-of-gravity energy of the state. We determine the transition frequency from the ground state to be 1276080105.5(1.2) MHz, corresponding to a center-of-gravity energy of 42565.45058(4) cm^{-1}. This result is a factor of 30 more precise than the previous best measurement and constitutes the most precise determination of an excited-state energy in a four-electron system to date. As theoretical methods advance, this result will enable stringent tests of quantum electrodynamics in four-electron systems.

DOI: 10.1103/8b1f-fpgq

I. INTRODUCTION

Over the past two decades, theoretical methods for four-electron atomic systems have advanced significantly. The most precise calculations to date, including quantum electrodynamics (QED) corrections for systems with four or more electrons, have employed explicitly correlated Gaussian (ECG) basis sets [1]. For the center-of-gravity energy of the $2s2p\ ^1P_1^o$ state, two high-precision theoretical predictions have been published [2,3]. Both incorporate QED effects and achieve uncertainties on the order of 300 MHz. For a recent overview of theoretical developments in light atomic systems, see Refs. [4,5].

In addition to energy-level calculations, the magnetic dipole (A) and electric quadrupole (B) hyperfine constants for this state were calculated to be $A = -13.8882(7)$ MHz and $B = 0.845\,40(4)$ MHz, respectively [6]. These values determine the hyperfine structure shown in Fig. 1. The isotope shift for this transition was also evaluated in Ref. [8].

Theoretical work has also addressed atomic properties beyond individual states. Notably, the nuclear quadrupole moment of the atom was independently calculated by two groups [9,10], providing an important benchmark for interpreting electric quadrupole interactions.

Experimentally, high-precision measurements of the $2s2p\ ^1P_1^o$ state in neutral ^{9}Be were reported by our group in 2018 [11], improving upon the pioneering results published by Johansson in 1963 [12] by more than two orders of magnitude. That work used a collimated beam of atomic beryllium and provided a key benchmark for testing atomic structure calculations, but its precision was limited to 40 MHz due to unresolved hyperfine structure. The result confirmed a theoretical prediction of the $2s2p\ ^1P_1^o$ energy by Puchalski *et al.* [2], which included α^6 QED corrections.

In 2024, our group published a study of the $2s3s\ ^1S_0$ state [13]. As part of that work, we also performed a second, less precise measurement of the $2s2p\ ^1P_1^o$ state energy using a dc discharge lamp as the atomic source. This measurement, with an uncertainty of 50 MHz, was intended as a test of the stability and reliability of the lamp-based approach. As the earlier work, its precision was limited by overlapping hyperfine structure.

This work improves upon the precision reported in previous studies by a factor of 30 by placing the experimental setup in a large magnetic field. The theoretical background, experimental design, and expected Zeeman shifts are described in Sec. II. The data analysis and results are presented in Sec. III, and the work is concluded in Sec. IV.

II. THEORY AND EXPERIMENTAL SETUP

Gaseous beryllium was produced in an argon gas-sustained dc discharge using a custom-built hollow cathode lamp. The lamp consists of two grounded stainless steel anodes flanking a central hollow cathode that contains a beryllium metal insert. The laser beams propagate along the axis of the lamp, passing through the center of the anodes and cathode. The

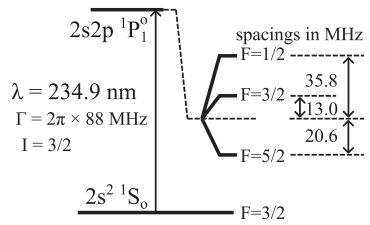

FIG. 1. A simplified energy-level diagram of the transition studied in this paper. The hyperfine splitting was calculated using the results from Puchalski *et al.* [6]. The natural linewidth of the transition is $\Gamma = 2\pi \times 88$ MHz [7], larger than the maximum separation of the hyperfine levels.

*Contact author: wraven@smith.edu

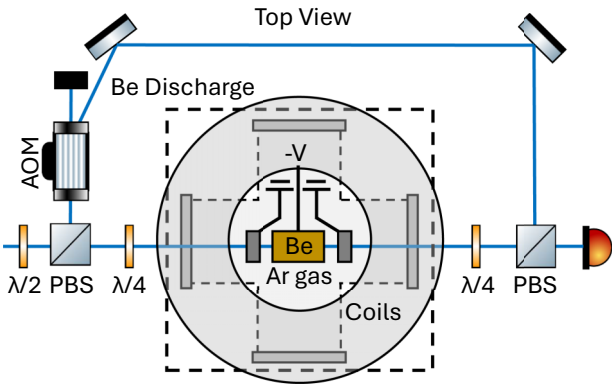

FIG. 2. A simplified diagram of the experimental setup. The pump beam is amplitude modulated using an acousto-optical modulator (AOM). The magnetic field is created by two coils, one above the vacuum system and one below, in a Helmholtz configuration. λ/2: half-wave plate; λ/4: quarter-wave plate; PBS: polarizing beam-splitter cube.

lamp design, whose dimensions are reported in Ref. [13], was based on earlier work [14,15] with minor modifications. A negative voltage was applied to the cathode using a Kepco BOP 500M power supply operating in constant current mode. Argon ions generated in the discharge were accelerated into the beryllium cathode, sputtering a small amount of neutral beryllium vapor into the lamp volume. The discharge could be initiated at pressures above 300 mTorr and sustained over a wide pressure range. Counterpropagating pump and probe beams were sent along the axis of the lamp in a saturated absorption spectroscopy configuration, as shown in Fig. 2. As discussed in Sec. III A, quarter-wave plates were inserted on both sides of the vacuum system. The *p*-polarized probe beam was converted to circular polarization before interacting with the atoms and then converted back to *p* polarization after passing through the second quarter-wave plate. Similarly, the *s*-polarized pump beam was converted to circular polarization before interacting with the atoms and then returned to *s* polarization. The pump beam was amplitude modulated at $f_{\mathrm{AM}} = 314.15$ kHz. After the interaction, the probe beam was detected by a photodetector and demodulated at f_{AM} using a lock-in amplifier (Stanford Research Systems SR865A). The output of the lock-in amplifier was recorded by a computer.

The laser frequency was measured and stabilized using a frequency comb (see Ref. [13] for details on the frequency control system). Briefly, the laser was locked to the frequency comb at a desired frequency. Data acquisition was paused for 60 ms, six times the lock-in amplifier's time constant, to allow the signal to settle. The output of the lock-in amplifier and the laser frequency were then recorded by the computer. The laser frequency was subsequently updated, and the process repeated.

In the absence of a magnetic field, the $2s2p\ ^1P_1^o$ state exhibits three hyperfine levels whose energy separation is smaller than the natural linewidth of the transition (see Fig. 1). When a magnetic field is applied, each magnetic sublevel experiences a Zeeman shift described by the interaction Hamiltonian $H = -\vec{\mu} \cdot \vec{B}$, where $\vec{\mu}$ includes contributions from both the electronic and nuclear magnetic dipole moments. The electronic Zeeman interaction dominates, but a small correction from the nuclear Zeeman effect is included in our modeling. These shifts lead to resolvable energy differences, as shown in Fig. 3. Since the $2s2p\ ^1P_1^o$ state is energetically well separated from other electronic configurations and the magnetic field used is not strong enough to significantly break down the *LS*-coupling scheme, effects such as magnetic-field-induced mixing with other configurations or *J*-*J* mixing are negligible. The model therefore only included the 12 sublevels of this manifold.We performed our measurements at a magnetic field of 400 G. This field was predicted from a model of the Helmholtz coils operating at 48 A and confirmed from our spectral fitting. The lower inset of Fig. 3(a) shows the symmetric Zeeman splitting of the ground state. The calculated slope of 598.277 Hz/G was obtained using the nuclear *g* factor measured by Nakamura *et al.* [16]. At 400 G, the maximum shifts come from the $m_F = \pm 3/2$ sublevels and is shifted by approximately ±360 kHz.

Figure 3(a) shows the calculated Zeeman splitting of the $2s2p\ ^1P_1^o$ state as a function of magnetic field. The zero-field hyperfine structure was calculated using the magnetic dipole and electric quadrupole hyperfine constants from Puchalski *et al.* [6]. As the magnetic field increases, four magnetic sublevels shift to higher frequency, four shift to lower frequency, and four converge toward the center of gravity. The upper inset of Fig. 3(a) shows the three distinct groupings that emerge at large magnetic fields. At large magnetic field, the four sublevels that shift to a higher frequency are well represented by $m_J = 1$, while the four that shift to a lower frequency are well represented by $m_J = -1$. The four sublevels in the middle are approaching 0 slope for the electronic contribution, which would then be well represented by $m_J = 0$. The details of the four sublevels near the center of gravity are shown in Fig. 3(b).

At 400 G, there is one cluster of real transitions centered around the center of gravity and two clusters symmetrically shifted by approximately ±560 MHz [see the upper inset of Fig. 3(a)]. In addition to the three clusters of real transitions, there are three crossover clusters between each pair of real transitions. The crossover between the two transition groupings at ±560 MHz will also appear near the center of gravity. However, as discussed in the next section, choosing appropriate polarization for the pump and probe beams can suppress this crossover, resulting in only a small residual feature. Therefore, we expect five spectral features, two clusters of real transitions near ±560 MHz with respect to the center of gravity, two clusters of crossover near ±270 MHz with respect to the center of gravity, and one spectral feature at the center of gravity created by a real transition and a small crossover. The separation between each spectral feature is large compared to the natural linewidth of 88 MHz.

Finally, in this experimental configuration, the laser propagation axis is perpendicular to the magnetic field axis. This arrangement was chosen due to experimental constraints. Each magnetic field coil consists of 90 turns of 4.5-mm-square wire, and the size and weight of the coils made a horizontal orientation less practical. Additionally, the laser operates at a wavelength of 234.9 nm, and for safety reasons, it is kept horizontal to the optical table. While the use of parallel axes is the typically used configuration, we found

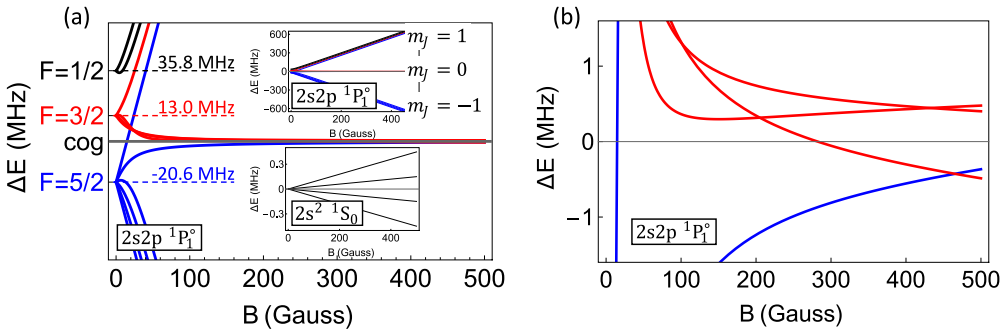

FIG. 3. (a) The main plot shows how the magnetic sublevels shift as a function of magnetic field to highlight how each magnetic sublevel shifts. The upper inset shows the same data over a broader vertical range to provide the overall structure: Four sublevels evolve into $m_J = +1$ states, four into $m_J = -1$ states, and four converge toward the center of gravity. The lower inset shows the splittings of the ground state. (b) A zoomed-in view of the four sublevels that converge near the center of gravity.

that inserting quarter-wave plates before and after the vacuum chamber produced spectra well suited for determining the center-of-gravity transition frequency with our perpendicular geometry.

To illustrate the impact of the magnetic field, Fig. 4 shows a representative spectrum recorded at zero magnetic field. In this case, the hyperfine components and crossovers are not resolved, as the hyperfine splittings are smaller than the natural linewidth of the transition. This lack of resolution limited the precision of previous measurements [11,13]. In contrast, the application of a strong magnetic field (see Fig. 5) lifts the degeneracy of the magnetic sublevels, allowing the center-of-gravity transition frequency to be extracted with much higher precision.

III. ANALYSIS AND RESULTS

A. A simplified model

At zero magnetic field, the magnetic sublevels are degenerate within each hyperfine state. In the presence of a nonzero magnetic field, this degeneracy is lifted. To extract the center-of-gravity transition frequency from the measured spectrum, we employ a simplified model based on several assumptions.

First, we assume the hyperfine structure is accurately described by the magnetic dipole and electric quadrupole constants calculated by Puchalski *et al.* with values of $A = -13.888\,2(7)$ MHz and $B = 0.845\,40(4)$ MHz, respectively [6]. Given the high correlation between the hyperfine constants and the spectral feature positions, fixing these theoretical values was essential to prevent an ill-conditioned fit, which leads to very large error bars on these parameters. With these constants fixed, only two free parameters remain in the model to determine the frequency of each spectral feature: the magnetic field strength and the center-of-gravity frequency. Importantly, the magnetic field is the only parameter to adjust the frequency spacing between the spectral features.

Second, we assume that certain groupings of magnetic sublevels are effectively degenerate. For example, at a magnetic field of 400 G, the four excited-state sublevels that shift to higher frequencies lie at 539.6, 553.3, 567.1, and 581.1 MHz above the center of gravity. Their spread of approximately 40 MHz is smaller than the natural linewidth

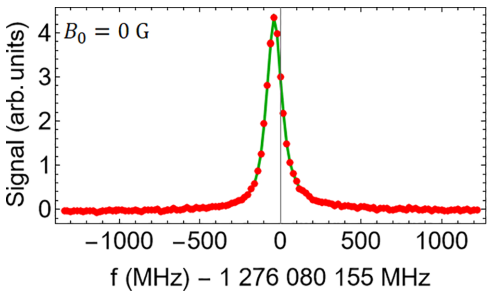

FIG. 4. Example spectrum collected at zero magnetic field. The hyperfine structure is unresolved due to the natural linewidth, $\Gamma = 2\pi \times 88$ MHz, being larger than the hyperfine splittings. In this graph, the green line is not a fit, but rather a line connecting the data points to guide the eye.

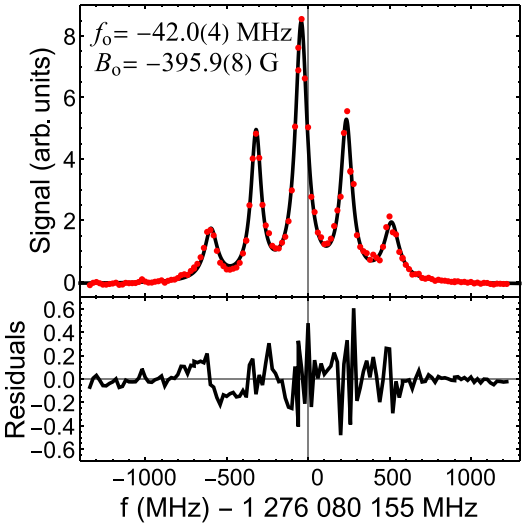

FIG. 5. An example spectrum collected using circularly polarized light for the pump and probe beam. For this spectrum, the argon pressure was 200 mTorr, the discharge voltage was −200 V, and the total laser power was 1.4 mW.

of 88 MHz. Given that transitions from the ground state are further complicated by nonparallel laser and magnetic field axes, quantum interference effects [5,17], unequal transition amplitudes, and overlapping crossovers, a full multicomponent fit would be unwieldy and unnecessary for the purposes of this analysis. Instead, we approximate these four sublevels as a single, degenerate state at their average frequency, in this case +560.3 MHz. Similarly, we treat the four sublevels that shift to lower frequency as a single degenerate state, whose values calculate to −580.8, −567.6, −553.7, and −539.0 MHz. Though the frequencies are not the negative of each other, the absolute value of the averages end up being the same to our precision, 560.3 MHz. It should be emphasized that the above numbers are given as an example for a 400 G field. In the fitting procedure, the magnetic field is a free parameter. Since the spacing between the spectral features depends on a single fit parameter, the magnetic field, the polarization of light is chosen to produce a symmetric spectrum.

We make the same degeneracy assumption for the four excited-state sublevels near the center of gravity and for the ground-state sublevels. The ground-state splitting is small and symmetric, and the excited-state sublevels span from −0.555 to +0.469 MHz relative to the center of gravity, with an average offset of just +10 kHz. This is well below our measurement precision.

These assumptions constrain our experimental setup. If the polarization of the light were to preferentially populate specific magnetic sublevels, for example, favoring the sublevels at 581.1 and −539.0 MHz, the frequency spacing between the most positive feature and the central feature would differ from the spacing between the central feature and the most negative feature. Because our model allows only a single fit parameter, the magnetic field, to determine the frequency spacing between features, the polarization of light is chosen to produce a symmetric spectrum in order to satisfy the model's assumptions.

Third, we assume that the spectral shape and amplitude of the central crossover between the ±560 MHz features does not affect our measurement. To validate this assumption, we performed measurements using different pump and probe beam polarizations that created symmetric spectra. The different polarizations change the amplitudes of the transitions and crossovers, but they did not result in a measurable change in the central feature's frequency within our final reported statistical uncertainty.

Further, we found that using circular polarization for the pump and probe beams produces spectra in which the real transitions near $f_{\mathrm{cog}} \pm 560$ MHz appear with reduced amplitude. As a result, the crossover between these two transitions should contribute only a small feature at the center of the spectrum, where the dominant signal arises from the real transition between the ground state and the four excited-state sublevels near the center of gravity (see Fig. 5).

Since the model simplifies the full atomic dynamics, we assign an uncertainty for the model. The scenario which would result in the largest measurement error would be that the central spectral feature's amplitude comes entirely from the transition from the highest ground-state sublevel (+360 kHz) to the lowest excited-state sublevel (−555 kHz). This would result in a maximum model error of 915 kHz. Based on these tests, we assign a conservative model uncertainty of 900 kHz to the center-of-gravity determination.

Based on this, we model the spectrum as the sum of five Lorentzian features: one central feature at the center of gravity, two representing the real transitions shifted furthest from the central feature near ±560 MHz, and two crossovers. The center frequencies of these components are calculated using the same two parameters introduced earlier: the magnetic field strength (nominally around 400 G) and the center-of-gravity frequency. The amplitude and width of each Lorentzian are treated as additional free parameters in the fit.

B. Systematic effects

External perturbations can shift atomic energy levels. In our experiment, we intentionally apply a large magnetic field to create a spectral feature centered on the center of gravity. However, other experimental parameters can induce small shifts in the measured transition frequencies. These include the background pressure from the argon gas, the discharge voltage, and the optical power of the pump and probe beams.

At low pressures, voltages, and laser powers, we assume that the resulting frequency shifts are linear. The measured center-of-gravity frequency can then be modeled as

$$f_{\mathrm{cog}}(P, V, s) = f_{\mathrm{cog}}(0, 0, 0) + m_P P + m_V V + m_s s, \qquad (1)$$

where $f_{\mathrm{cog}}(P, V, s)$ is the experimentally measured center-of-gravity frequency for a given pressure P, discharge voltage V, and total laser power s. The unknown parameters are the unperturbed center-of-gravity frequency $f_{\mathrm{cog}}(0, 0, 0)$ and the linear slopes m_P, m_V, and m_s corresponding to each systematic variable. To determine these parameters, we recorded spectra at various settings: argon pressures between 180 and 700 mTorr, discharge voltages between −250 and −480 V, and total laser powers between 0.7 and 3.3 mW. These ranges were chosen to maintain adequate signal-to-noise ratios while probing a wide range of conditions. The lamp was found to be unstable below approximately −200 V, so data below this threshold were excluded.

For each set of systematic parameters, three to five scans were taken. A total of 112 scans were included in this analysis. For each scan, the center-of-gravity frequency and magnetic field were extracted. A least-squares fit to Eq. (1) was performed to determine the model parameters. We find the following slope values for the systematic shifts $m_P = -7.2(8)$ kHz/mTorr, $m_V = -23.4(1.4)$ kHz/V, $m_s = 0.16(12)$ kHz/mW. The statistical uncertainty on the extracted center-of-gravity frequency was determined to be 800 kHz. The best value was found to be 1 276 080 105.5 MHz.

In addition to frequency shifts arising from external fields, there is also uncertainty associated with imperfect alignment between the pump and probe beams. To estimate this effect, the pump beam was intentionally misaligned in various directions until the amplitude of the saturated absorption signal was reduced by approximately 50%. A total of 25 scans were recorded with different spatial misalignments. Following the methodology in Refs. [18,19], the mean shift in the extracted

TABLE I. Summary of experimental uncertainties contributing to the determination of the center-of-gravity frequency. All values are 1σ uncertainties.

Source of uncertainty	Uncertainty (kHz)
Statistical uncertainty from fits	800
Pump-probe beam misalignment	200
Frequency comb calibration	10
Model approximation	900
Total uncertainty (quadrature sum)	1200

TABLE II. Comparison of experimental and theoretical values for the center-of-gravity frequency $f_{\rm cog}$ of the $2s2p\,^1P_1$ state in neutral ^{9}Be.

Year	Expt./Theory	$f_{\rm cog}$ (MHz)	E (cm^{-1})
2013	Theory [2]	1 276 079 820(330)	42 565.441(11)
2018	Expt. [11]	1 276 080 090(40)	42 565.4501(13)
2021	Theory [3]	1 276 079 880(270)	42 565.443(9)
2024	Expt. [13]	1 276 080 115(50)	42 565.4509(17)
2025	Expt. (this work)	1 276 080 105.5(1.2)	42 565.450 58(4)

center frequency across these scans was divided by a factor of 5, and this value was taken as the uncertainty due to pump-probe beam misalignment. This contribution was found to be 200 kHz. The alignment uncertainty is mostly negligible compared to the statistical and model uncertainties.

Finally, the uncertainty in the laser frequency, determined by the accuracy of the frequency comb, was negligible at the 10 kHz level. A summary of all experimental uncertainties is presented in Table I.

IV. SUMMARY AND OUTLOOK

The final result of this work is a center-of-gravity frequency of $f_{\rm cog} = 1\,276\,080\,105.5(1.2)$ MHz, corresponding to a center-of-gravity energy of 42 565.450 58(4) cm^{-1} for the $2s2p\,^1P_1^o$ state in neutral ^{9}Be. This result is a factor of 30 more precise than the previous best measurement and represents the most precise determination of an excited-state energy in a four-electron system to date. A comparison of recent experimental and theoretical progress is provided in Table II. Our experimental precision now reaches better than 1.5% of the natural linewidth, providing a benchmark value for future theoretical calculations. For this broad transition, further improvements in precision will require greater control over the atomic environment.

Experimentally, the next step will be to revisit recent measurements of the $2s3d\,^1D_2$ [20] and $2s3s\,^1S_0$ [13] states. Both transitions were previously limited in precision by overlapping hyperfine structure, and should benefit significantly from spectroscopy in a strong magnetic field. Further improvements in precision for this four-electron system are also possible using the weak intercombination line $2s^2\,^1S_0 \rightarrow 2s2p\,^3P_1$, which has an extremely narrow linewidth of $\Gamma = 2\pi \times 0.067$ Hz [7]. With experimental uncertainties now reaching parts-per-billion accuracy, the stage is set for high-accuracy theory to meet this benchmark, providing a stringent test of atomic structure and QED in multielectron systems.

ACKNOWLEDGMENT

This work was supported by the National Science Foundation through Grants No. PHY-2319917 and No. PHY-2110311.

DATA AVAILABILITY

The data that support the findings of this article are openly available [21].

[1] J. Mitroy, S. Bubin, W. Horiuchi, Y. Suzuki, L. Adamowicz, W. Cencek, K. Szalewicz, J. Komasa, D. Blume, and K. Varga, Theory and application of explicitly correlated Gaussians, Rev. Mod. Phys. **85**, 693 (2013).

[2] M. Puchalski, J. Komasa, and K. Pachucki, Testing quantum electrodynamics in the lowest singlet states of the beryllium atom, Phys. Rev. A **87**, 030502(R) (2013).

[3] S. Nasiri, L. Adamowicz, and S. Bubin, Benchmark calculations of the energy spectra and oscillator strengths of the beryllium atom, J. Phys. Chem. Ref. Data **50**, 043107 (2021).

[4] I. Hornyák, L. Adamowicz, and S. Bubin, Ground and excited ^1S states of the beryllium atom, Phys. Rev. A **100**, 032504 (2019).

[5] K. J. Ahrendsen, C. Maruko, K. R. Albert-Aranovich, Q. Berfield-Brewer, A. Esseln, L. Guo, A. E. Ishimwe, Y. Kuzniar, A. E. McKenna, K. J. Soto Villarreal, A. Uprety, L. V. da Silva, K. F. Vogt, and W. D. Williams, Absolute frequency measurement of the $2p^2(^3P)3s\,^2P \rightarrow 2p^2(^3P)3p\,^2D^o$ transitions in neutral ^{14}N, Phys. Rev. A **108**, 042815 (2023).

[6] M. Puchalski, J. Komasa, and K. Pachucki, Fine and hyperfine splitting of the low-lying states of ^{9}Be, Phys. Rev. A **104**, 022824 (2021).

[7] A. Kramida, Yu. Ralchenko, J. Reader, and NIST ASD Team, NIST Atomic Spectra Database (ver. 5.12) (online), available https://physics.nist.gov/asd (20 April 2025) (National Institute of Standards and Technology, Gaithersburg, MD, 2024).

[8] M. Puchalski, K. Pachucki, and J. Komasa, Isotope shift in a beryllium atom, Phys. Rev. A **89**, 012506 (2014).

[9] M. Puchalski, J. Komasa, and K. Pachucki, Hyperfine structure of the 2^3P state in ^{9}Be and the nuclear quadrupole moment, Phys. Rev. Res. **3**, 013293 (2021).

[10] Y.-S. Zhang, W. Dang, K. Wang, and Y.-B. Tang, Revisiting the hyperfine interval for the $2s2p\,^3P_J$ state in ^{9}Be, Phys. Rev. A **111**, 042819 (2025).

[11] E. C. Cook, A. D. Vira, C. Patterson, E. Livernois, and W. D. Williams, Testing quantum electrodynamics in the lowest sin-

glet state of neutral beryllium-9, Phys. Rev. Lett. **121**, 053001 (2018).
[12] L. Johansson, Spectroscopy, Ark. Fys. **23**, 119 (1963).
[13] K. J. Ahrendsen, T. Karani, and W. D. Williams, Precision measurement of the absolute energy of the $2s3s\,^1S_0$ state in neutral ^{9}Be, Phys. Rev. A **110**, 032818 (2024).
[14] V. K. Saini, P. Kumar, K. K. Sarangpani, S. K. Dixit, and S. V. Nakhe, Development of a see-through hollow cathode discharge lamp for (Li/Ne) optogalvanic studies, Rev. Sci. Instrum. **88**, 093101 (2017).
[15] I. A. Sulai and P. Mueller, Laser spectroscopy of metastable palladium at 340 and 363 nm, Phys. Rev. A **102**, 042805 (2020).
[16] T. Nakamura, M. Wada, K. Okada, I. Katayama, S. Ohtani, and H. A. Schuessler, Precision spectroscopy of the Zeeman splittings of the $^9Be^+2^2S_{1/2}$ hyperfine structure for nuclear structure studies, Opt. Commun. **205**, 329 (2002).
[17] R. C. Brown, S. Wu, J. V. Porto, C. J. Sansonetti, C. E. Simien, S. M. Brewer, J. N. Tan, and J. D. Gillaspy, Quantum interference and light polarization effects in unresolvable atomic lines: Application to a precise measurement of the ^{6,7}Li ^{6,7}Li D_2 lines, Phys. Rev. A **87**, 032504 (2013).
[18] C.-M. Wu, T.-W. Liu, M.-H. Wu, R.-K. Lee, and W.-Y. Cheng, Absolute frequency of cesium $6S$–$8S$ 822 nm two-photon transition by a high-resolution scheme, Opt. Lett. **38**, 3186 (2013).
[19] M. T. Herd, E. C. Cook, and W. D. Williams, Absolute frequency measurement of the $6D_{5/2}$ level of neutral ^{133}Cs using two-photon spectroscopy, Phys. Rev. A **104**, 042812 (2021).
[20] E. C. Cook, A. D. Vira, and W. D. Williams, Resonant two-photon spectroscopy of the $2s3d\ ^1D_2$ level of neutral ^{9}Be, Phys. Rev. A **101**, 042503 (2020).
[21] https://doi.org/10.5281/zenodo.15548297.